Journal of the European Ceramic Society 41 (2021) 380–388

Contents lists available at ScienceDirect

Journal of the European Ceramic Society

journal homepage: www.elsevier.com/locate/jeurceramsoc

Polymer-derived Biosilicate-C composite foams: Phase development and photothermal effect

Fulden Dogrul [a,b,*], Stefano Bortolin [b], Davide Del Col [b], Nicola Dengo [c,d], Danilo Pedron [c], Martin Michalek [a], Hamada Elsayed [b,e], Dušan Galusek [a,f], Enrico Bernardo [b]

[a] FunGlass – Centre for Functional and Surface Functionalized Glass, Alexander Dubcek University of Trenčín, Trenčín, Slovakia
[b] Department of Industrial Engineering, Università degli Studi di Padova, Padova, Italy
[c] Department of Chemical Sciences (DiSC), Università degli Studi di Padova, Padova, Italy
[d] Science and High Technology Department and To.Sca.Lab, University of Insubria, Como, Italy
[e] Refractories, Ceramics and Building Materials Department, National Research Centre, 12622, Cairo, Egypt
[f] Joint Glass Centre of the IIC SAS, TnU AD and FChFT STU, Trenčín, Slovakia

ARTICLE INFO

Keywords:
Biosilicate® glass-ceramic
Polymer-derived-ceramics
SiOC
Composites
Photo-thermal effect

ABSTRACT

Glass-ceramic matrix composites for bone-tissue regeneration were produced in the form of highly porous foams utilizing the 'polymer-derived ceramics' (PDCs) approach. More precisely, two different commercial silicone polymers (a poly-methyl-siloxane, MK, and a polymethyl-phenyl-silsesquioxane, H44), reacting with suitable Na_2O, CaO, and P_2O_5 yielding fillers were considered. The reaction was designed to yield products resembling Biosilicate® glass-ceramic i.e. $Na_2CaSi_2O_6$ embedded in a silico-phosphate glass matrix. Subsequently, the samples were heat treated either in the air or in the N_2 atmosphere, implying improvements in the mechanical properties and providing extra functionality. The pyrolysis in an inert atmosphere led to composites comprising a carbon phase, which promoted the absorption of infrared radiation. Such functionality makes the obtained composites promising in the perspective of disinfection of bone-tissue implants and photothermal therapy.

1. Introduction

Bioactive materials are a class of materials able to bond themselves to living tissues. The bioactive glass invented by Hench termed Bioglass® (also 45S5) is based on a composition of 45 % SiO_2, 24.5 % Na_2O, 24.5 % CaO, and 6.0 % P_2O_5 (in wt%) and since its discovery it represented a revolutionary bioactive material. In particular, it features the highest bioactivity index, defined as the reciprocal time taken for more than half of the interface to connect to the bone [1,2].

The first sign of bioactivity of the materials is the formation of hydroxyl carbonated apatite (HCA), formed at the interface between living tissue and bioactive material when the material is in contact with simulated body fluid (SBF) or implanted into the human body. However, since bioactive glasses show low mechanical strength and fracture toughness, the application areas of these glasses are limited to the repair of non-load-bearing bone defects. To overcome these limitations and combine key features such as the high bioactivity and good mechanical properties (i.e., strength, toughness, and hardness) in one material, bioactive glass-ceramics have been developed [3–5].

The effect of crystallization on the HCA layer formation in bioactive glass-ceramics is not fully understood. While one study suggested that in vitro HCA layer formation depended on the proportion of residual glass (over 90 %) in the crystallized Bioglass® 45S5 [5], other studies proved that crystallization of Bioglass®, even in the case of full crystallization, did not obstruct HCA layer formation, but simply delayed it [6,7]. The commercial bioactive glass-ceramics such as Ceravital®, Bioverit® and A/W (apatite/wollastonite) Cerabone® all exhibit improved mechanical properties (i.e., crushing strength, flexural strength, and Young's modulus) compared to 45S5, but their bioactivity level is relatively low. Their bioactivity index is below 8, comparable to that of traditional calcium phosphate ceramics but significantly lower than 12.5 of Bioglass® [8].

Nearly two decades ago, the first bioactive glass-ceramic developed by Peitl et al. [7], featured both good mechanical properties and high bioactivity index. This material, like 45S5, belonged to the SiO_2-CaO--Na_2O-P_2O_5 system, but exhibited a crystallinity degree from 30 to 65 vol %. The main phase consisted of $Na_2Ca_2Si_3O_9$, with phosphorus ions included in solid solution and/or in the residual glass phase [7]. A highly

* Corresponding author at: FunGlass – Centre for Functional and Surface Functionalized Glass, Alexander Dubcek University of Trenčín, Trenčín, Slovakia.
E-mail address: fulden.dogrul@tnuni.sk (F. Dogrul).

https://doi.org/10.1016/j.jeurceramsoc.2021.09.012
Received 9 June 2021; Received in revised form 18 August 2021; Accepted 4 September 2021
Available online 9 September 2021

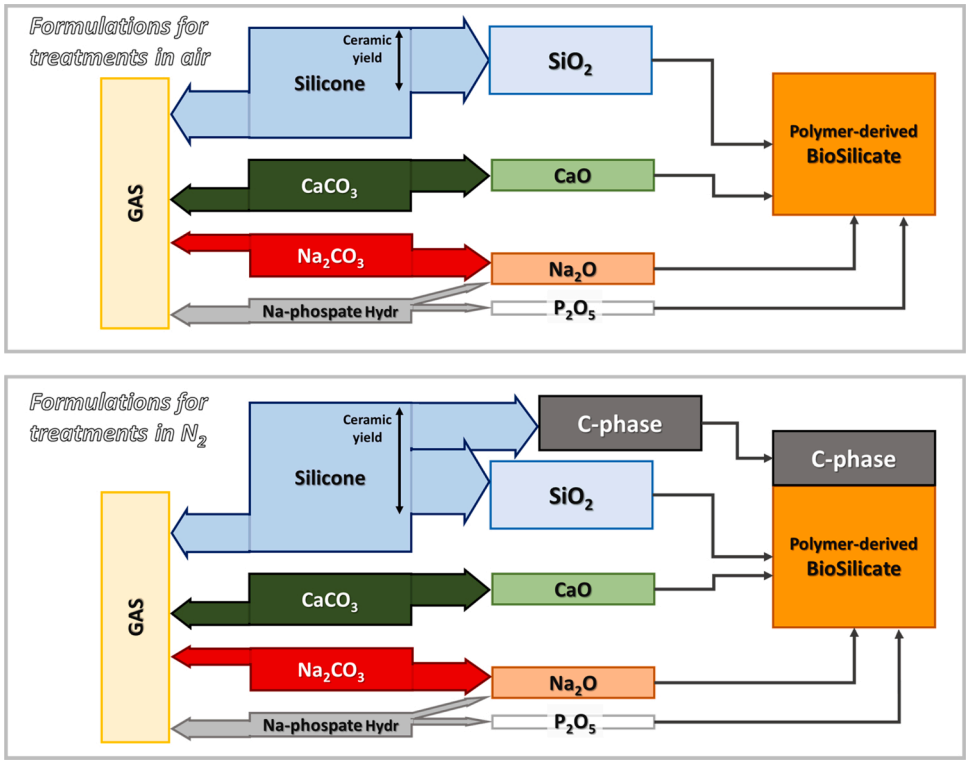

Fig. 1. Concept of polymer-derived Biosilicate systems, without or with extra C-based phase.

bioactive glass-ceramic based on the same system, but with about 99.5 % crystallinity, was later developed by Ravagnani et al. and patented as Biosilicate® glass-ceramic in 2003 [9]. The composition again is very similar to that of Bioglass®, being 23.75 % Na_2O-23.75 % CaO-48.5 % SiO_2-4.0 % P_2O_5 (wt%). The biologic properties of Biosilicate® glass-ceramic, such as osteoconductivity, osteoinductivity, biocompatibility and antibacterial effect are comparable to that of Bioglass® [10,11]. The production of Biosilicate® glass-ceramics, in the form of granules, powders or monoliths, is currently established on a commercial scale [12].

Elsayed et al. [13] recently proposed an alternative 'glass-free' route to develop Biosilicate® glass-ceramics based on preceramic polymers. The oxidative decomposition of silicone resins provides amorphous silica, which reacts easily with micro- and nano-sized fillers (e.g. carbonates, hydroxides or oxides) yielding phase pure products at low temperature (900−1100 °C). Biosilicate® glass-ceramics represent just an extension of an approach already successfully applied to polycrystalline biosilicates, such as wollastonite ($CaSiO_3$), diopside ($CaMgSi_2O_6$), åkermanite ($Ca_2MgSi_2O_7$), hardystonite ($Ca_2ZnSi_2O_7$) and various solid solutions [14–17].

Borate and phosphate fillers, which form a liquid phase upon firing were found to catalyse the phase development by favouring ionic interdiffusion, providing an opportunity for preparation of 'polymer-derived glass-ceramics'. In the specific case of silicone-derived Biosilicate® material [13], the phosphate filler forms a phosphate-enriched glass phase surrounding Na-Ca silicate crystals. Strictly speaking, the term 'glass-ceramic' is not nominally appropriate, since the product does not originate from a homogeneous glass [18]. However, it may be considered as such, due to the strict similarity of its mineralogical composition with real Biosilicate® glass-ceramic [13].

One of the most important advantages of polymer-derived glass-ceramics is the feasibility of polymer-shaping processes, including modern additive manufacturing technologies [13–15,17,19]. A component is first shaped in the polymeric state, and then it is subjected to thermal transformation. Such transformation may lead to additional shaping opportunities, related to the gas release from both fillers and preceramic polymers. In particular, hydrated borate and phosphate fillers decompose into their anhydrous variants at low temperature (<350 °C), i.e. with silicones in form of viscous pastes. The silicone matrix can be thus easily foamed in a first step of thermal treatment, also causing the cross-linking (which in turn implies the 'freezing' of the cellular structure determined by the release of water vapour bubbles), before experiencing ceramization at higher temperatures [13,16]. Hydrated phosphates and borates may be considered as 'double-active' fillers since they release water vapour as a foaming agent, and form a glass forming melt at higher temperature.

A relatively unexploited opportunity to fabricate biomaterials from preceramic polymers is the formation of a carbon phase 'in situ'. Carbon polymorphs are becoming increasingly interesting for improving osteogenic differentiation [20] and for the functionalization of biomaterials [21–25]. The high absorption properties, especially in the near infrared range (NIR), encourage the use of carbon materials, such as graphene oxide, carbon nanotubes, carbon nanohorns, carbon dots, graphene dots and fullerenes [26–31] for cancer photothermal therapy/photodynamic therapy (PTT/PDT) [32]. Apart from the therapy of tumors, the local overheating of C-based materials can be applied also in disinfection [33]. In the specific case of silicones, pyrolytic, graphene-like carbon is typically formed by thermal treatment in inert atmosphere (nitrogen or argon). More precisely, silicones yield a silicon oxycarbide (SiOC) nanocomposite, with free carbon included in a silica-based matrix, and featuring some Si-C bonds along with Si-O bonds [34,35].

So far, only a few studies reported on the multiple role of silicones in shaping of porous components and yielding both silica as the bioceramic matrix, and carbon, as a secondary functional phase. Fu et al. [36] and Zhu et al. [37] focused on relatively simple systems consisting of larnite (Ca_2SiO_5) and forsterite (Mg_2SiO_5), respectively. In terms of bioactivity the two silicate systems are promising, but still far from 45S5 Bioglass® and Biosilicate®.

The present study is dedicated to the exploration of Biosilicate-mimicking foams derived from two different silicone polymers (poly-

Table 1
Batch formulations for polymer-derived Biosilicate foams.

Oxides in Biosilicate® [wt%]	Oxide quantities (g) referred to 10 g of SiO_2 in Biosilicate®		Source quantities (g) referred to 10 g of SiO_2 /source	
			Firing in Air	*Firing in N_2*
SiO_2 [48.5%]	*10*		11.90 / MK 18.90 / H44	15.66 / MK [of which 3.15 as extra C-phase] 26.05 / H44 [of which 8.75 as extra C-phase]
P_2O_5 [4%]	*0.82*	*0.72*	4.13 / Hydrated Na-phosphate	
Na_2O [23.75%]	*4.90*	*4.18*	7.14 / Na_2CO_3	
CaO [23.75 %]	*4.90*		8.74 / $CaCO_3$	

methyl-silsesquioxane and poly-methyl-phenyl-silsesquioxane), differing mainly in the yield of carbon-based phase, upon treatment in nitrogen. The effectiveness of free carbon in promoting photo-thermal effects was confirmed by simple tests with an IR lamp. Treatment in air was performed for a systematic comparison of mechanical properties of the developed materials. The concept of formulations for treatments in air (with silicone acting simply as a source of silica) and in nitrogen is summarized by Fig. 1.

2. Experimental procedure

2.1. Starting materials

Two commercial solid silicone resins, MK (poly-methyl-siloxane) and H44 (poly-methyl-phenyl-silsesquioxane), were used as silica precursors. These polymers (both from Wacker-Chemie GmbH, Munich, Germany) provided a ceramic yield of 84 wt.% (MK) and 53 wt.% (H44), after firing in air, and 84 wt.% (MK) and 72 wt.% (H44), after firing in N_2 at 1000 °C. When treated in air, the ceramic residue consisted of pure silica (SiO_2), whereas it corresponded to a SiOC nanocomposite, after treatment in N_2. Calcium carbonate ($CaCO_3$, <10 μm, Bitossi, Vinci, Italy), sodium carbonate (Na_2CO_3, <10 μm, Sigma-Aldrich, Germany) and hydrated sodium phosphate ($Na_2HPO_4{\cdot}12H_2O$, <10 μm, Sigma-Aldrich, Germany) were used as active fillers.

2.2. Direct foaming experiments

Both silicone resins (33 vol%) were dissolved in isopropyl alcohol (C_3H_8O, 2-Propanol, HPLC BASIC, Scharlau, Scharlab Italia srl, Riozzo di Cerro al Lambro, Italy) in a glass beaker and then the $CaCO_3$, Na_2CO_3, and $Na_2HPO_4{\cdot}12H_2O$ powders were added. The amounts of fillers were adjusted with respect to the silica content from the polymers, to match the exact $SiO_2/P_2O_5/Na_2O/CaO$ balance of Biosilicate® glass-ceramic, as reported in Table 1. It can be noted that hydrated sodium phosphate accounted for the content of P_2O_5; the amount of Na_2CO_3 as a source of Na_2O had to be adjusted, to account for the amount of Na_2O introduced from the phosphate salt (see also Fig. 1). The obtained suspensions were homogenized using a mechanical mixer (Argo Lab AM20-D, Giorgio Bormac s.r.l, Modena, Italy), operating at 350 rpm, for 90 min. MK- and H44-based pastes were cast into Al moulds and foamed at 350 °C for 30 min in air. Demoulded samples (after an expansion of approximately 100 vol%) were finally fired either in air or in flowing nitrogen at a heating rate of 1 °C/min, with holding stages at 500 °C, for 3 h, and 1000 °C for 1 h. The fired samples were then cooled down to room temperature in the furnace at a rate of 5 °C/min. The firing schedule was based on previous results [13].

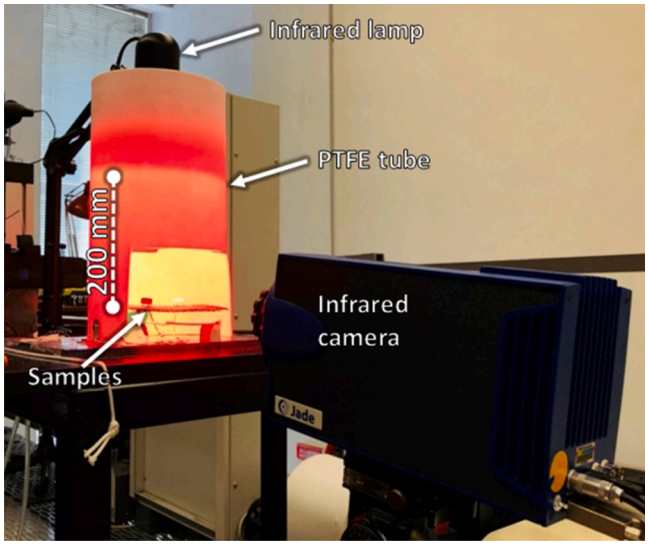

Fig. 2. Experimental set-up for the assessment of photothermal effect.

2.3. Characterization

A digital calliper was used to measure the dimensions of all samples after the heat treatment. A helium pycnometer (Micromeritics AccuPyc 1330, Norcross, GA) was used to determine the apparent and true density of the obtained foams. Scanning electron microscopy (SEM, FEI Quanta 200 ESEM, Eindhoven, Netherlands), equipped with energy dispersive spectroscopy (EDS), was used to perform the microstructural characterizations of the samples.

The samples were subjected to compression tests (Quasar 25, Galdabini, Cardano, Italy), operating with a crosshead speed of 1 mm min^{-1}. Each data point represents an average value obtained by testing at least five specimens. Mineralogical analysis was performed on powdered samples utilizing X-ray diffraction (XRD, Bruker AXS D8 Advance, Bruker, Germany), supported by the Match! program package (Crystal Impact GbR, Bonn, Germany).

Selected polymer-derived Biosilicate®-like samples, in powder form, were further studied by Raman spectroscopy. The spectra were collected with a homemade micro-Raman system with a single 320 mm focal length imaging spectrograph (Triax-320, Horiba Jobin Yvon, Edison, NJ, USA) equipped with a holographic 1800 g/mm grating and a liquid-nitrogen-cooled CCD detector (Spectrum One, ISA Instruments Jobin-Yvon Spex, Edison, NJ, USA). The excitation source was a Spectra-Physics Ar^+ laser (Stabilite 2017-06S, Spectra-Physics, Mountain View, CA, USA) operating at 514.5 nm, and an appropriate long-pass edge filter (Semrock Filters, IDEX Health & Science, LLC, Rochester, NY, USA) was used to reduce the stray-light level. An optical microscope (Olympus BX 40, Olympus Co., Tokyo, Japan), equipped with three objectives, 20X/0.35, 50X/0.75 and 100X/0.90, optically coupled to the spectrograph, was used to record the Raman spectra in micro configuration.

The same powders were characterized in terms of their sensitivity to infrared radiation. Both powdered samples and bulk foams were tested. Diffuse reflectance spectra of the powder samples were acquired using a Cary 5E UV–vis-NIR double-beam spectrometer (Agilent, Santa Clara, CA, USA) equipped with a diffuse reflectance accessory. The spectra were acquired in the wavelength range from 2500 nm to 300 nm with a step of 1.111 nm (SBW 2.000 nm). The spectrometer was operated in a fixed signal/noise-ratio mode with an acceptable signal/noise level of 1000 and a timeout of 5 s. The spectra were corrected for the 100 % R level (using a flat PTFE reference plate) and the 0% R level (using a light trap).

Selected foam samples were placed inside a cylindrical

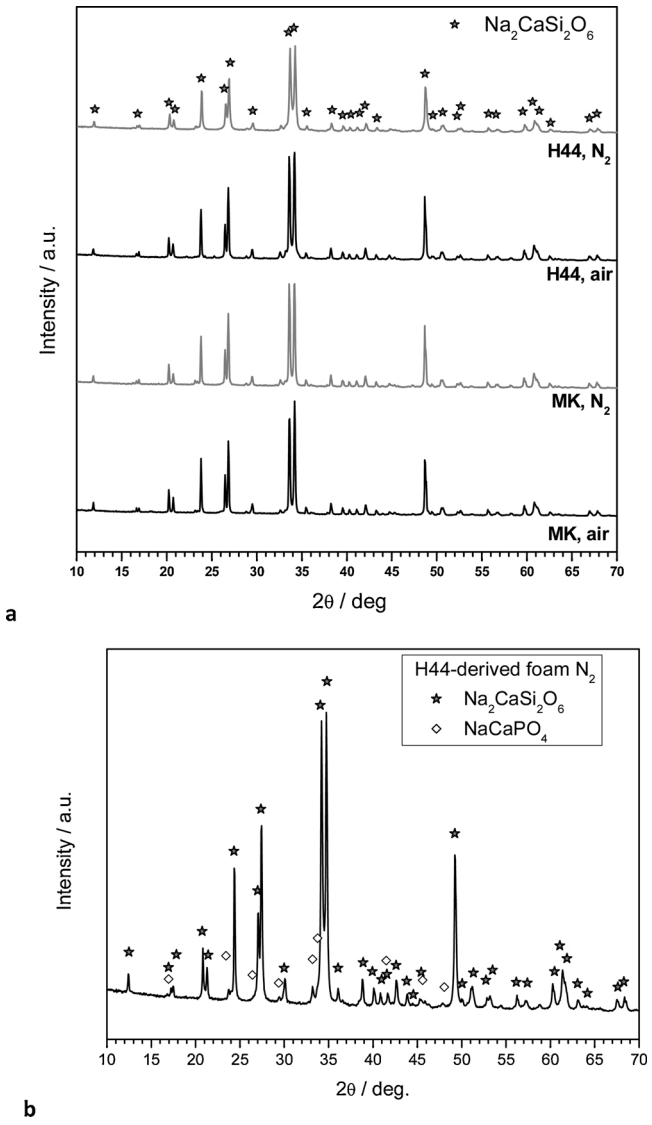

Fig. 3. Mineralogical analysis of polymer-derived Biosilicate foams: a) comparison of foams from different silicone resins and formulation/atmosphere; b) detailed analysis of H44-derived foam fired in N_2.

polytetrafluoroethylene (PTFE) tube, as illustrated by Fig. 2, supported by four small pins connected to a metallic grid. The cylindrical tube provides a uniform background for the infrared camera whereas the pins and the metallic grid minimize thermal conduction from the samples to the surroundings. A commercial incandescent IR-lamp (Philips R95, Eindhoven, The Netherlands) was placed at the centre of the tube, at a distance of 200 mm from the supporting grid. The PTFE tube had a front opening allowing the observation of samples by an infrared camera (Jade 3 MWIR Cedip Infrared Systems, Croissy-Beaubourg, France). The internal temperature of each sample was measured by inserting a T-type thermocouple through a small hole (1 mm diameter, 3 mm depth) drilled at the centre of each tested sample. Conductivity paste was also used to provide thermal contact between the sensor and the sample. The reference cold junction of the thermocouples was maintained at 0 °C using an automatic ice-point reference. The uncertainty of the temperature measured with thermocouples is equal to ±0.5 °C. During the tests, thermocouples readings and IR-images were collected with a frequency of 1 Hz.

The tests started with two samples at the same (ambient) temperature. The IR-lamp was switched on and temperatures were measured until a steady state was reached: in this situation, the samples were in thermal equilibrium. Then the lamp was turned off and the temperature of both the samples was monitored until the ambient temperature was reached again.

Table 2
Details on gas evolution in polymer-derived Biosilicate materials.

Sample	Nominal weight loss (wt%)	Relative weight losses (%)		
		Decomposition of phosphate	Ceramic conversion	Decomposition of carbonates
MK - air	*35.4*	*22.9*	*16.8*	*60.2*
MK - N_2	*33.4*	*21.8*	*21.1*	*57.1*
H44 - air	*47.0*	*14.2*	*48.7*	*37.2*
H44 - N_2	*36.2*	*15.5*	*43.9*	*40.6*

3. Results and discussion

One of the main aims of the present investigation was the assessment of the flexibility of polymer-derived ceramics approach in yielding products resembling Biosilicate® glass-ceramics. Previous experiments had been dedicated simply to MK and H62C commercial silicones, modified by the inclusion of oxide fillers, and thermally treated in air [13]. The used liquid methyl-phenyl polysiloxane H62C had led to foams with a remarkable strength-to-density ratio (crushing strength of ~3 MPa, at a porosity of ~75 vol%), but not fully comparable to actual Biosilicate® glass-ceramics in terms of phase assemblage. The typical main phase ($Na_2CaSi_2O_6$, i.e., $Na_2O{\cdot}CaO{\cdot}2SiO_2$) was less pronounced in the diffraction pattern. The foams prepared from the MK polymer had lower strength but strictly resembled Biosilicate® glass-ceramics in phase composition. The XRD patterns shown in Fig. 3 confirm the similarity of phase composition also for the H44-based foams fired in air.

The selection of precursors (Table 1) was essentially aimed at controlling the chemical composition of the glass-ceramic products. The fillers, however, had also an impact on the shaping of highly porous foams. Considering a reference quantity of 10 g of SiO_2, Biosilicate (as the sum of characteristic oxides, in appropriate balance) amounted to 20.6 g. The supply of 10 g SiO_2 in the form of the MK polymer for firing in air required the addition of 11.9 g of polymer, with 1.9 g representing the weight loss during thermal treatment. Hydrated sodium phosphate precursor yielded all P_2O_5 and part of Na_2O, with a related loss of 2.59 g, in the form of water vapour. Na- and Ca-carbonates provided the rest of Na_2O and all CaO, with the loss of 6.8 g of CO_2. The overall weight loss could be then estimated as 1.9 g + 2.59 g + 6.8 g = 11.29 g, which accounts for 35 wt.% of the weight of the used raw materials. Single contributions could be easily calculated from the ratio between single loss/total loss. For the same MK-based system fired in air, as an example, the relative weight loss related to Na-phosphate was 2.59/(11.29)= ~0.23 = 23 wt%. Table 2 summarizes the calculations for all formulations.

Besides the differences in the overall gas release (from 33 to 47 wt%), there were also substantial differences among formulations. The decomposition of carbonates was dominant in MK-based formulations, whereas the ceramic conversion was more significant in H44-based samples (related to the lower ceramic yield of H44 compared to MK silicone resin). The effects overlap significantly: Na_2CO_3 is known to decompose at 326 °C [38], whereas the adopted phosphate salt undergoes dehydration at 350 °C [13] and H44 releases moieties below 300 °C even by itself [39].

All compositions led to macroporous foams already at 350 °C. Besides this, the cellular structure was further formed during thermal treatment, due to the gas evolution at temperatures above 350 °C. In the samples fired in air, this led to samples with multimodal porosity (Fig. 4). Unlike foams from liquid silicone H62C [13,14,16], the

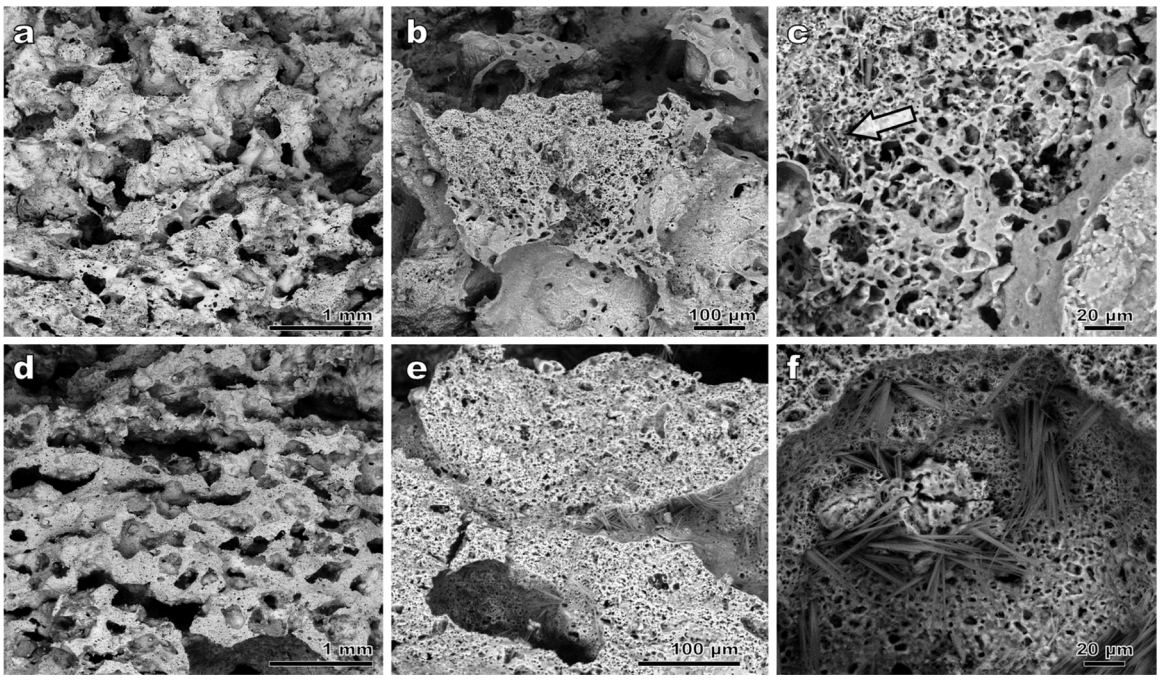

Fig. 4. Microstructural details polymer-derived Biosilicate foams fired in air: a-c) MK-derived; d-f) H44-derived.

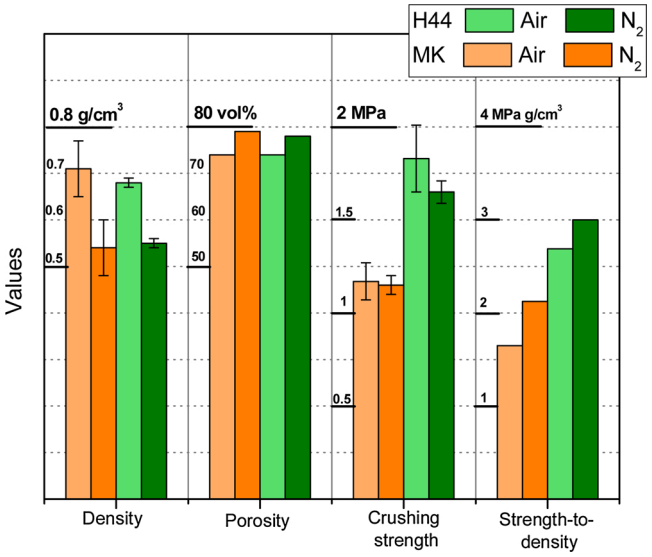

Fig. 5. Overview of properties of polymer-derived Biosilicate foams.

homogeneity of MK-derived foams was poor. However, wide 'channels' visible already before firing (Fig. 4a) were complemented by micro-porous struts (Fig. 4b). Such hierarchical porosity is particularly appreciable in modern biomaterials, where they enhance material/cells/body fluid interactions [40]. Finally, the cavities of 'micro--foamed' struts contained some fibrous crystals (Fig. 4c, see arrow), attributable to the main sodium-calcium silicate crystal phase.

As summarized in Fig. 5, the newly prepared MK-derived foams, fired in air, had a crushing strength (1.2 ± 0.1 MPa) not statistically different from that of MK-derived foams developed previously (1.6 ± 0.5 MPa) [13], with a similar, completely open overall porosity (~75 %). H44-derived foams, fired in air, were generally stronger (crushing strength of 1.8 ± 0.1 MPa) and compared well with foams from sintered Biosilicate® glass-ceramic powder, manufactured by gel casting [41]. The improvement cannot be interpreted as the result of a more homogenous cellular structure, since the foam contained quite coarse cell walls (Fig. 4d). A key difference, in our opinion, was represented by the extensive development of interlocked fibrous crystals inside porous struts (Fig. 4e), often protruding from cell walls (Fig. 4f).

Additional evidence of the flexibility of the approach, in terms of preparation of Biosilicate®-like glass-ceramics were provided by treatment of the mixture in flowing nitrogen. The formulations for treatment in air (Table 1), were simply based on the different ceramic yield of the two used polymers. When treated in air, the ceramic residue consists of just amorphous silica; when treated in nitrogen, the polymers transformed into SiOC ceramic residues with two different stoichiometries.

According to Scheffler et al. [42], upon transformation in inert atmosphere the MK resin yields the ceramic residue with the atomic proportions 31.6 %Si-48.1 %O-20.2 %C ($Si_3O_{4.56}C_{1.92}$), while for H44 resin the atomic proportions are 18.7 %Si-28.7 %O-52.6 %C ($Si_3O_{4.6}C_{8.45}$). As mentioned above, SiOC is recognized as a nano-composite with turbostratic carbon nano-sheets dispersed in silica-based glass, with the presence of Si-C bonds in siloxane network. In a homogeneous system heat treated above 1200 °C SiC may separate from silica [43]. In the present case, according to previous experiments on polymer-derived silicates [13,16] silica was expected to react with oxide fillers well below 1200 °C, so that an early phase separation could occur. In this perspective, the molecular formulae of polymer-derived SiOC could be re-written as follows:

MK-derived SiOC: $Si_3O_{4.56}C_{1.92} \leftrightarrow 2.28\ SiO_2 + 0.72\ SiC + 1.2\ C$

H44-derived SiOC: $Si_3O_{4.\ 6}C_{8.45} \leftrightarrow 2.3\ SiO_2 + 0.7\ SiC + 7.75\ C$

In the batches reported in Table 1, the relative amounts of silicones and oxide fillers for the development of the desired Biosilicate system were calibrated according to the silica fraction of SiOC. The rest of the ceramic residue was thus intended to stay 'inert' and possibly provide extra phases (SiC and C), in different amounts (see Fig. 1).

For MK, the nominally inert part of the ceramic residue corresponded to ~13 wt% of the final composite. In fact, as observed previously, for a reference quantity of 10 g of SiO_2, Biosilicate®-like component amounted to 20.6 g; the 10 g of SiO_2 added in the form of the MK polymer, implied parallel addition of 3.15 g of C-phase, i.e. 3.15/(20.6 + 3.15)=~0.13 = 13 wt%. The inert part originating from the H44

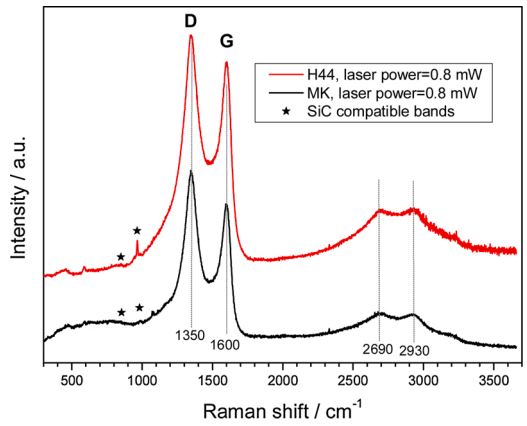

Fig. 6. Raman spectra of MK- and H44-derived Biosilicate foams fired in N_2.

polymer amounted to ~30 wt%, using analogous estimation.

The formation of Si-C bonds is not straightforward. The presence of fillers yielding silicate phases may cause deviations from the atomic proportions reported above. According to ^{29}Si NMR spectroscopy studies on polymer-derived silicate systems fired in N_2 [17], the detection of SiO_3C, SiO_2C_2 and $SiOC_3$ units was uncertain, due to the overlapping of signals with those of silicate crystals. Moreover, XPS studies evidenced free carbon as the most recognizable C-based phase [17]. However, for the sake of clarity, the Si-O-C atomic proportions mentioned above were kept as a reference.

Fig. 3a shows that the MK-derived product treated in N_2 did not differ significantly from that prepared in air. Despite the expected presence of other phases the typical main phase ($Na_2CaSi_2O_6$, i.e., $Na_2O{\cdot}CaO{\cdot}2SiO_2$) of Biosilicate® glass-ceramics was confirmed. No diffraction maxima could be assigned to SiC. For the H44-derived foams fired in N_2, the $Na_2CaSi_2O_6$ phase was also confirmed again, but a reduction in the intensity of diffraction maxima was observed. This was quite consistent with the enhanced content of extra phases yielded by heat treatment of H44. The reduction in intensity could be seen as an effect of a more pronounced formation of C-rich amorphous phase. More detailed analysis of H44-derived foam (Fig. 3b), confirmed the formation of $Na_2CaSi_2O_6$, accompanied by low intensity diffraction lines attributable to $NaCaPO_4$ (PDF#76-1456), similarly to those found in the '2P' variant of Biosilicate® glass-ceramics [13].

The presence of a C-based phase was monitored by Raman spectroscopy (Fig. 6). For both used polymers, the spectra are consistent with the formation of 'turbostratic' carbon, i.e. graphite-like carbon in which graphene layers are parallel to each other, but with some level of disorder in the plane direction. The characteristic 'first-order' bands, i.e. D and G bands at 1360 and 1580 cm^{-1}, respectively, were clearly visible. 'Second-order' bands between 2700 and 2900 cm^{-1} [44], were also detected. Deviations from the theoretical positions (e.g. upshifting of G band) were attributed to silicon doping [45]. The marked asymmetry of the D band was interpreted as the result of the contributions from silicate crystals, namely Si–O stretching vibrations of SiO_4 groups with 4, 3 and 2 bridging oxygens (Q_4, Q_3, and Q_2 species), which are known to provide Raman bands near 1180, 1080 and 1000 cm^{-1}, respectively [46]. Although not detectable by X-ray diffraction, the presence of SiC nano-crystallites cannot be excluded, especially for the H44-derived sample, as indicated by the band at 960 cm^{-1} (bands at 860 and 959 cm^{-1} correspond to transverse optical (TO) and longitudinal optical (LO) Raman modes of SiC) [47].

The foams fired in N_2 were lighter than those fired in air, but they were also much stronger. As shown in Fig. 5, the strength-to-density ratio of the H44-based foams fired in N_2 nearly doubled in comparison to the MK-based foams fired in air. As previously observed for other polymer-derived silicate systems, the increase of mechanical properties could be attributed to a ceramic transformation (not implying the

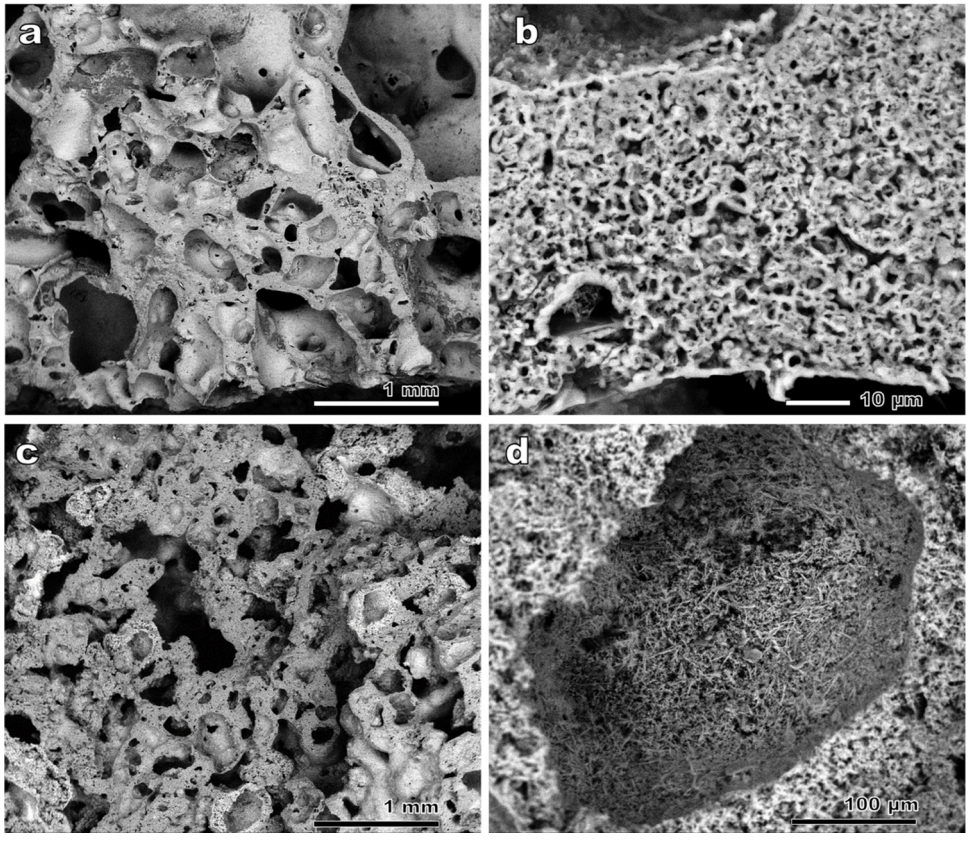

Fig. 7. Microstructural details of polymer-derived PDC Biosilicate-like foams fired in nitrogen: a, b) MK-derived; c, d) H44-derived.

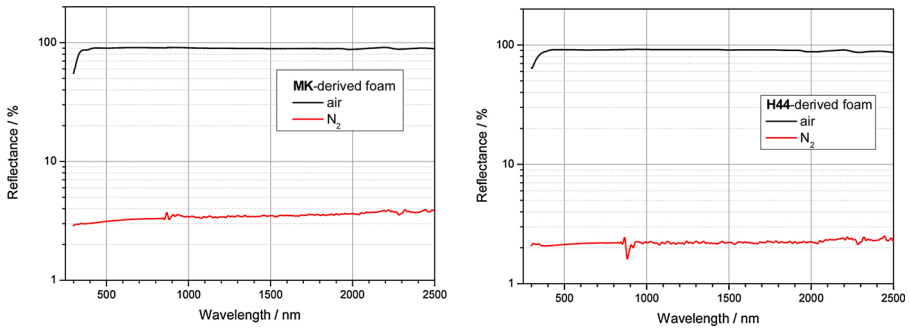

Fig. 8. Diffuse reflectance spectra of MK- and H44-based Biosilicate foams, fired in air and N_2.

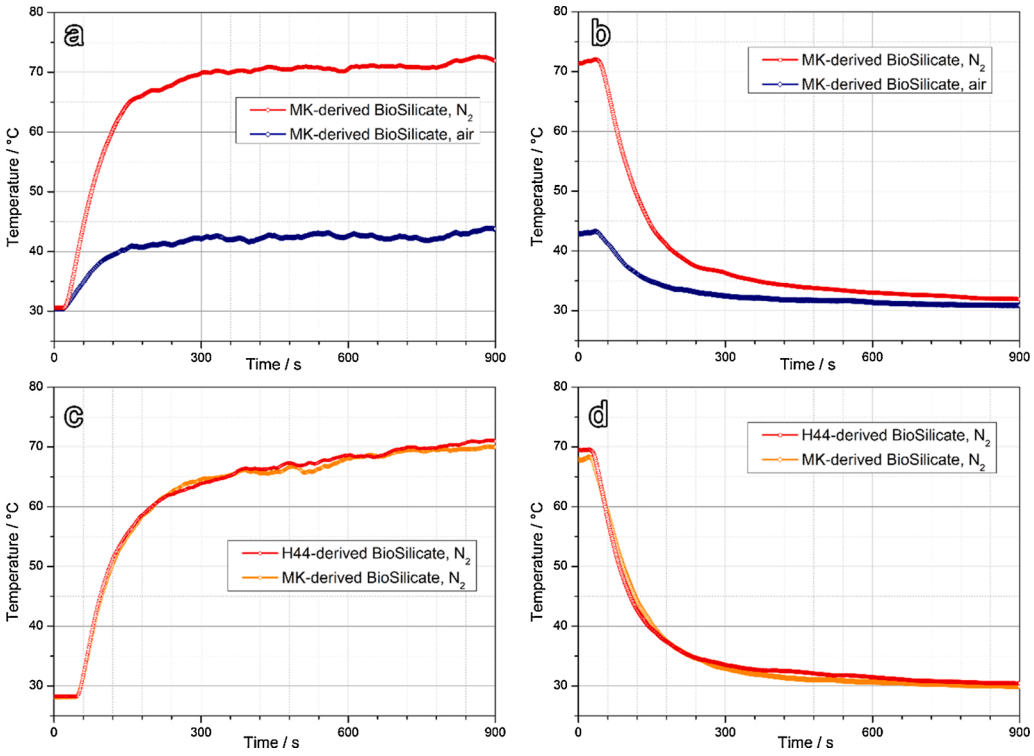

Fig. 9. Evolution of internal temperature of polymer-derived Biosilicate foam samples: MK-based samples fired in air and in N_2 during heating (a) and cooling (b) phases; MK- and H44-based samples fired in N_2 during heating (c) and cooling (d) phases.

strongly exothermic oxidation of Si-CH_3 bonds) leading to reduced internal stresses [16] rather than to other microstructural features. The MK-derived foams (Fig. 7a) were less uniform than those prepared from H44 (Fig. 7c). Again, the struts were quite 'spongy' (Fig. 7b), fulfilling the condition of hierarchical porosity. Fibrous crystal formation was also confirmed, as demonstrated by detailed SEM images of cell walls (Fig.7d).

The presence of amorphous carbon is attractive from the point of view of functionalization of prepared foams, particularly the effectiveness of photothermal effect. Diffuse reflectance spectroscopy (DRS) measurements were performed to assess the absorption properties of the samples in the UV–vis-NIR range from 300 to 2500 nm (Fig. 8). Both MK- and H44-derived samples fired in air showed a similarly high reflectance, which was stable at about 89–90 % in the whole measured range. Only two weak features at 2283 and 2001 nm were observed. The sharp decrease in reflectance observed below 400 nm can be ascribed to the low-wavelength part of the material absorption edge. Conversely, the N_2 treated samples were characterized by a very low reflectance over the whole measured spectral range, with some interesting features. The recorded reflectance values ranged from 2.9 % to 3.8 % for the MK-derived sample, and from 2.0%–2.3% for the H44-derived sample. The DRS showed the striking effect of the presence of the carbon sheets in the material, which turns from a very poor Vis-NIR absorber to a remarkably strong one. The detected broadband light absorption finds analogies with extremely absorbing coatings featuring the carbon nano-structures -mentioned above [48].

The remarkable absorption of infrared radiation at relatively high wavelengths is a fundamental condition for the assessment of photothermal effect not stimulated by high power lasers, operating at λ=~860 nm [36,37], but by a commercial, low-cost incandescent lamp (power = 100 W), with an emission peak at λ=~1000 nm [49].

Fig. 9 shows the results of two infrared-lamp heating tests. Temperatures measured with the mini-thermocouples located inside the samples are plotted against time. The upper part reports the comparison between MK-derived samples fired in air and in nitrogen, in both heating (Fig. 9a, with infrared lamp turned on) and cooling (Fig. 9b, with infrared lamp turned off) phases. The lower part shows a comparison between MK- and H44-derived samples, both fired in nitrogen, again during heating (Fig. 9c) and cooling (Fig. 9d) phases. Furthermore, for a selected time step (625 s during the heating phase, with lamp turned

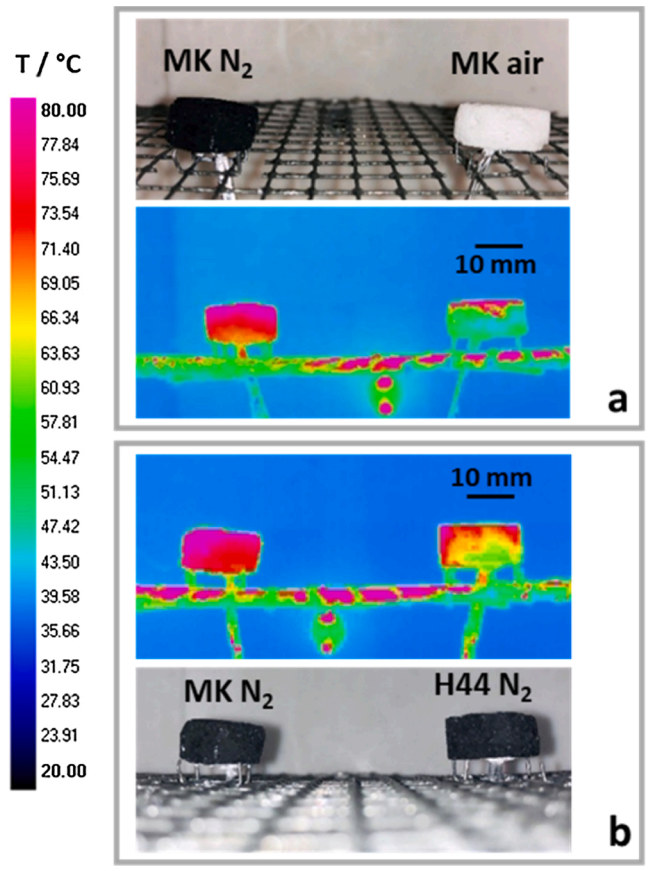

Fig. 10. Temperature maps of polymer-derived Biosilicate foam samples after 625 s under infrared irradiation (lamp on): a) MK-based samples fired in air and in N_2; b) MK- and H44-based samples fired in N_2.

on), Fig. 10 reports the temperature fields on the surface of the samples obtained by the infrared camera.

It is evident that the inclusion of C-based phase in the MK-derived samples led to an enhanced heating (C-containing sample was by 30 °C hotter than the sample fired in air; Fig. 9a). In both samples fired in nitrogen, a rapid heating (Fig. 9c) up to about 70 °C was observed, independently from the carbon content. The maximum temperature was maintained for approximately 1 min (with lamp off, Fig. 9b and d), before progressive cooling due to natural convection and radiative heat transfer towards the external ambient. The maximum temperature achieved upon IR irradiation is particularly important: as reported by Xu et al. [50], common bacteria are disinfected upon heating above 55 °C (as in the present case), due to the heat shock denaturisation of proteins. Both tested samples passed this threshold in less than 3 min. The adopted IR wavelength is also interesting, since it is comprised in a range (between 700–1400 nm), for which light has a good capacity to penetrate mammalian bodies while causing minimal damage to normal tissues [50].

It should be noted that the heating/cooling curves were determined by thin thermocouples placed at the centre of each sample. In the samples fired in air the infrared camera detected temperatures well above 60 °C only at the surface directly exposed to the lamp (Fig. 10a), while most of the surface underwent intensive heating for the C-containing bodies (Fig. 10b).

In conclusion, silicone polymers and fillers have a huge potential for developing products resembling glass-ceramics by direct ceramization, with well-established tissue engineering applications and an extra functional carbon phase. Future efforts will be undoubtedly dedicated to further extensions, e.g. in the additive manufacturing of silicone/fillers mixtures, with the objective of mimicking Biosilicate® glass-ceramics and providing a carbon-based secondary phase. The possible use of H44 is very promising: whereas MK may be easily applied to the manufacturing of polymer-derived scaffolds (fired only in air) by direct ink writing [13–15,17], H44 may be blended with photocurable acrylic resins, enabling the application of more refined stereolithography approaches [19]. Some efforts will be undoubtedly aimed at a systematic assessment of the biological response, without and/or under irradiation with infrared light, to confirm biocompatibility, bioactivity and the potential for photothermal therapy.

4. Conclusions

The mixing of silicone resin with oxide fillers was confirmed as a promising way for the development of products resembling Biosilicate® glass-ceramics by polymer derived route. The approach enabled both the shaping of highly porous foams and the obtainment of the desired phase assemblage, independently from the starting silicone polymer. A further opportunity, consisting of the exploitation of silicones as sources of both reactive silica and turbostratic carbon, was evidenced for the first time, in a Biosilicate-like system, for treatments in nitrogen atmosphere. The extra C-phase in the polymer-derived Biosilicate-like samples fired in nitrogen induced photothermal effect: the feature can be utilized in therapy and disinfection, and could be activated by a conventional infrared lamp.

Declaration of Competing Interest

The authors declare that they have no known competing financial interests or personal relationships that could have appeared to influence the work reported in this paper.

Acknowledgments

This paper is a part of the dissemination activities of the project FunGlass (Centre for Functional and Surface Functionalized Glass). This project has received funding from the European Union's Horizon 2020 research and innovation programme under grant agreement No. 739566. Discussions with Prof. A. R. Boccaccini (University of Erlangen-Nuremberg, Germany), scientific board member (Biomaterials) of the Centre for Functional and Surface Functionalized Glass, are greatly acknowledged.

References

[1] L.L. Hench, The story of Bioglass®, J. Mater. Sci. Mater. Med. 17 (2006) 967–978, https://doi.org/10.1007/s10856-006-0432-z.
[2] W. Cao, L.L. Hench, Bioactive materials, Ceram. Int. 22 (1996) 493–507, https://doi.org/10.1016/0272-8842(95)00126-3.
[3] L.L. Hench, T. Kokubo, Properties of bioactive glasses and glass-ceramics, in: J. Black, G. Hastings (Eds.), Handbook of Biomaterial Properties., Springer, Boston, MA, 1998, https://doi.org/10.1007/978-1-4615-5801-9_22.
[4] L.L. Hench, R.J. Splinter, W.C. Allen, T.K. Greenlee Jr., Bonding mechanisms at the interface of ceramic prosthetic materials, J. Biomed. Mater. Res. 5 (1971) 117–141, https://doi.org/10.1002/jbm.820050611.
[5] P. Li, Q. Yang, F. Zhan, T. Kokubo, The effect of residual glassy phase in a bioactive glass-ceramic on the formation of its surface apatite layer in vitro, J. Mater. Sci. Mater. Med. 3 (1992) 452–456, https://doi.org/10.1007/BF00701242.
[6] O. Filho Peitl, G.P. La Torre, L.L. Hench, Effect of crystallization on apatite-layer formation of bioactive glass 45S5, J. Biomed. Mater. Res. 30 (1996) 509–514, https://doi.org/10.1002/(SICI)1097-4636(199604)30:4<509::AID-JBM9>3.0.CO;2-T.
[7] O. Peitl, E. Dutra Zanotto, L.L. Hench, Highly bioactive $P_2O_5 \pm Na_2O \pm CaO \pm SiO_2$ glass-ceramics, Non. Cryst. Solids 292 (2001) 115–126, https://doi.org/10.1016/S0022-3093(01)00822-5.
[8] J. Massera, Bioactive glass-ceramics: from macro to nano. Nanostructured Biomaterials for Regenerative Medicine, Woodhead Publishing, 2020, pp. 275–292, https://doi.org/10.1016/B978-0-08-102594-9.00010-3.
[9] J. Moura, L.N. Teixeira, C. Ravagnani, O. Peitl, E.D. Zanotto, M.M. Beloti, H. Panzeri, A.L. Rosa, P.T. de Oliveira, In vitro osteogenesis on a highly bioactive glass-ceramic (Biosilicate), J. Biomed. Mater. Res. 82 (2007) 545–557, https://doi.org/10.1002/jbm.a.31165.

[10] S.M. Brandão, S.A. Schellini, A.D. Moraes, C.R. Padovani, C.H. Pellizzon, O. Peitl, E.D. Zanotto, Biocompatibility analysis of bioglass® 45S5 and biosilicate® implants in the rabbit eviscerated socket, Orbit 31 (2012) 143–149, https://doi.org/10.3109/01676830.2011.648798.
[11] M.C. Crovace, M.T. Souza, C.R. Chinaglia, O. Peitl, E.D. Zanotto, Biosilicate® — a multipurpose, highly bioactive glass-ceramic. In vitro, in vivo and clinical trials, J. Non. Solids 432 (2016) 90–110, https://doi.org/10.1016/j.jnoncrysol.2015.03.022.
[12] M. Montazerian, E.D. Zanotto, History and trends of bioactive glass-ceramics, J. Biomed. Mater. Res. A. 104 (2016) 1231–1249, https://doi.org/10.1002/jbm.a.35639.
[13] H. Elsayed, P. Rebesan, M.C. Crovace, E.D. Zanotto, E. Bernardo, Biosilicate® scaffolds produced by 3D-printing and direct foaming using preceramic polymers, J. Am. Ceram. Soc. 102 (2019) 1010–1020, https://doi.org/10.1111/jace.15948.
[14] S. Fu, M. Zhu, Y. Zhu, Organosilicon polymer-derived ceramics: an overview, J. Advan. Ceram. 8 (2019) 457–478, https://doi.org/10.1007/s40145-019-0335-3.
[15] H. Elsayed, M. Sinico, M. Secco, F. Zorzi, P. Colombo, E. Bernardo, B-doped hardystonite bioceramics from preceramic polymers and fillers: synthesis and application to foams and 3D-printed scaffolds, J. Eur. Ceram. Soc. 37 (2017) 1757–1767, https://doi.org/10.1016/j.jeurceramsoc.2016.12.002.
[16] H. Elsayed, M. Secco, F. Zorzi, K. Schuhlade, R. Detsch, A.R. Boccaccini, E. Bernardo, Highly porous polymer-derived bioceramics based on a complex hardystonite solid solution, Materials 12 (2019) 3970, https://doi.org/10.3390/ma12233970.
[17] L. Fiocco, S. Agnoli, D. Pedron, M. Secco, S. Tamburini, L. Ferroni, C. Gardin, B. Zavan, E. Bernardo, Wollastonite-diopside-carbon composite foams from a silicone resin and inorganic fillers, Ceram. Int. 44 (2018) 931–937, https://doi.org/10.1016/j.ceramint.2017.10.025.
[18] A. Dasan, H. Elsayed, J. Kraxner, D. Galusek, E. Bernardo, Hierarchically porous 3D-printed akermanite scaffolds from silicones and engineered fillers, J. Eur. Ceram. Soc. 39 (2019) 4445–4449, https://doi.org/10.1016/j.jeurceramsoc.2019.06.021.
[19] J. Deubener, M. Allix, M.J. Davis, A. Duran, T. Höche, T. Honma, T. Komatsu, S. Krüger, I. Mitra, R. Müller, S. Nakane, M.J. Pascual, J.W.P. Schmelzer, E. D. Zanotto, S. Zhou, Updated definition of glass-ceramics, J. Non. Solids 501 (2018) 3–10, https://doi.org/10.1016/j.jnoncrysol.2018.01.033.
[20] A. Dasan, H. Elsayed, J. Kraxner, P. Colombo, E. Bernardo, Engineering of silicone-based mixtures for the digital light processing of akermanite scaffolds, J. Eur. Ceram. Soc. 40 (2020) 2566–2572, https://doi.org/10.1016/j.jeurceramsoc.2019.11.087.
[21] D. Shao, M. Lu, D. Xu, X. Zheng, Y. Pan, Y. Song, J. Xu, M. Li, M. Zhang, J. Li, G. Chi, L. Chen, B. Yang, Carbon dots for tracking and promoting theosteogenic differentiation of mesenchymal stem cells, Biomater. Sci. 5 (2017) 1820–1827, https://doi.org/10.1039/C7BM00358G.
[22] N. Saito, Y. Usui, K. Aoki, N. Narita, M. Shimizu, K. Hara, N. Ogiwara, K. Nakamura, N. Ishigaki, H. Kato, S. Taruta, M. Endo, Carbon nanotubes: biomaterial applications, Chem. Soc. Rev. 38 (2009) 1897–1903, https://doi.org/10.1039/B804822N.
[23] N. Ogihara, Y. Usui, K. Aoki, M. Shimizu, N. Narita, K. Hara, K. Nakamura, N. Ishigaki, S. Takanashi, M. Okamoto, H. Kato, H. Haniu, N. Ogiwara, N. Nakayama, S. Taruta, N. Saito, Biocompatibility and bone tissue compatibility of alumina ceramics reinforced with carbon nanotubes, Nanomedicine 7 (2012) 981–993, https://doi.org/10.2217/NNM.12.1.
[24] S. Shafiei, M. Omidi, F. Nasehi, H. Golzar, D. Mohammadrezaei, M.R. Rad, A. Khojasteh, Egg shell-derived calcium phosphate/carbon dot nanofibrous scaffolds for bone tissue engineering: fabrication and characterization, Mater.Sci. Eng.C. 100 (2019) 564–575, https://doi.org/10.1016/j.msec.2019.03.003.
[25] C. Wu, L. Xia, P. Han, M. Xu, B. Fang, J. Wang, J. Chang, Y. Xiao, Graphene-oxide-modified β-tricalcium phosphate bioceramics stimulate in vitro and in vivo osteogenesis, Carbon 93 (2015) 116–129, https://doi.org/10.1016/j.carbon.2015.04.048.
[26] K. Yang, L. Hu, X. Ma, S. Ye, L. Cheng, X. Shi, C. Li, Y. Li, Z. Liu, Multimodal imaging guided photothermal therapy using functionalized graphene nanosheets anchored with magnetic nanoparticles, Adv.Mater. 24 (2012) 1868–1872, https://doi.org/10.1002/adma.201104964.
[27] A.L. Antaris, J.T. Robinson, O.K. Yaghi, G. Hong, S. Diao, R. Luong, H. Dai, Ultra-low doses of chirality sorted (6,5) carbon nanotubes for simultaneous tumor imaging and photothermal therapy, ACS Nano 7 (2013) 3644–3652, https://doi.org/10.1021/nn4006472.
[28] J.R. Whitney, S. Sarkar, J. Zhang, T. Do, T. Young, M.K. Manson, T.A. Campbell, A. A. Puretzky, C.M. Rouleau, K.L. More, D.B. Geohegan, C.G. Rylander, H.C. Dorn, M. N. Rylander, Single walled Carbon Nanohorns as photothermal cancer agents, Lasers Surg. Med. 43 (2011) 43–51, https://doi.org/10.1002/lsm.21025.
[29] M. Zheng, Y. Li, S. Liu, W. Wang, Z. Xie, X. Jing, One-pot to synthesize multifunctional carbon dots for near infrared fluorescence imaging and photothermal cancer therapy, ACS Appl. Mater. Interfaces 8 (2016) 23533–23541, https://doi.org/10.1021/acsami.6b07453.
[30] F. Wo, R. Xu, Y. Shao, Z. Zhang, M. Chu, D. Shi, S. Liu, A multimodal system with synergistic effects of magneto-mechanical, Photothermal, photodynamic and chemo therapies of Cancer in graphene-quantum dot-coated hollow magnetic nanospheres, Theranostics 6 (2016) 485–500, https://doi.org/10.7150/thno.13411.
[31] V. Krishna, A. Singh, P. Sharma, N. Iwakuma, Q. Wang, Q. Zhang, J. Knapik, H. Jiang, S.R. Grobmyer, B. Koopman, B. Moudgil, Polyhydroxy fullerenes for non-invasive Cancer imaging and therapy, Small 6 (2010) 2236–2241, https://doi.org/10.1002/smll.201000847.
[32] J. Yu, L. Yang, J. Yan, W.C. Wang, Y.-C. Chen, H.-H. Chen, C.-H. Lin, Carbon nanomaterials for photothermal therapies. Carbon Nanomaterials for Bioimaging, Bioanalysis, and Therapy, John Wiley & Sons Ltd, 2018, pp. 309–340, https://doi.org/10.1002/9781119373476.ch12.
[33] S. Han, J. Sun, S. He, M. Tang, R. Chai, The application of graphene-based biomaterials in biomedicine, Am. J. Transl. Res. 11 (2019) 3246–3260. PMID: 31312342; PMCID: PMC6614642.
[34] K. Lu, Porous and high surface area silicon oxycarbide-based materials - A review, Mater. Sci. Eng. R Rep. 97 (2015) 23–49, https://doi.org/10.1016/j.mser.2015.09.001.
[35] C. Stabler, E. Ionescu, I. Gonzalo-juan, M. Graczyk-zajac, Silicon oxycarbide glasses and glass - ceramics : "all - Rounder" materials for advanced structural and functional applications, J. Am. Ceram. Soc. 101 (2018) 4817–4856, https://doi.org/10.1111/jace.15932.
[36] S. Fu, H. Hu, J. Chen, Y. Zhu, S. Zhao, Silicone resin derived larnite / C scaffolds via 3D printing for potential tumor therapy and bone regeneration, Chem. Eng. J. 382 (2020), 122928, https://doi.org/10.1016/j.cej.2019.122928.
[37] T. Zhu, M. Zhu, Y. Zhu, Fabrication of forsterite scaffolds with photothermal-induced antibacterial activity by 3D printing and polymer-derived ceramics strategy, Ceram. Int. 46 (2020) 13607–13614, https://doi.org/10.1016/j.ceramint.2020.02.146.
[38] V. Siriwardane Ranjani, A. Poston James, C. Robinson, T. Simonyi, Effect of additives on decomposition of sodium carbonate: precombustion CO_2 capture sorbent regeneration, United States. 25 (2011), https://doi.org/10.1021/ef101486m.
[39] C. Ohl, M. Kappa, V. Wilker, Novel open-cellular glass foams for optical applications, J. Am. Ceram. Soc. 94 (2011) 436–441, https://doi.org/10.1111/j.1551-2916.2010.04121.x.
[40] C. Minas, D. Carnelli, E. Tervoort, A.R. Studart, 3D printing of emulsions and foams into hierarchical porous ceramics, Adv. Mater. 28 (2016) 9993–9999, https://doi.org/10.1002/adma.201603390.
[41] E. Bernardo, H. Elsayed, A.R. Romero, M.C. Crovace, E.D. Zanotto, T. Fey, Biosilicate® glass-ceramic foams from refined alkali activation and gel casting, Front. Mater. 7 (2021) 411, https://doi.org/10.3389/fmats.2020.588789.
[42] M. Scheffler, T. Takahashi, J. Kaschta, H. Muensted, P. Buhler, P. Greil, Pyrolytic decomposition of preceramic organo polysiloxanes, in: Innovative Processing and Synthesis of Ceramics, Glasses, and Composites IV: Ceramic Transactions, 115, 2000, pp. 239–250.
[43] A. Saha, R. Raj, D.L. Williamson, A model for the nanodomains in polymer-derived SiCO, J. Am. Ceram. Soc. 86 (2006) 2188–2195, https://doi.org/10.1111/j.1551-2916.2006.00920.x.
[44] E. López-Honorato, P.J. Meadows, R.A. Shatwell, P. Xiao, Characterization of the anisotropy of pyrolytic carbon by Raman spectroscopy, Carbon 48 (2010) 881–890, https://doi.org/10.1016/j.carbon.2009.11.010.
[45] Z. Wang, P. Li, Y. Chen, J. Liu, W. Zhang, Z. Guo, M. Dongb, Y. Li, Synthesis, characterization and electrical properties of silicon-doped graphene films, J. Mater. Chem. C Mater. Opt. Electron. Devices 3 (2015) 6301–6306, https://doi.org/10.1039/C5TC00563A.
[46] J. You, G. Jiang, K. Xu, High temperature Raman spectra of sodium disilicate crystal, glass and its liquid, J. Non-Crys. Solids 282 (2001) 125–131, https://doi.org/10.1016/S0022-3093(01)00335-0.
[47] M. Dragomir, M. Valant, M. Fanetti, Y. Mozharivskyj, A facile chemical method for the synthesis of 3C–SiC nanoflakes, RSC Adv. 6 (2016) 21795–21801, https://doi.org/10.1039/C6RA00789A.
[48] L.J. Lehman, C. Yung, N. Tomlin, D. Conklin, M. Stephens, Carbon nanotube-based black coatings, Appl. Phys. Rev. 5 (2018), 11103, https://doi.org/10.1063/1.5009190.
[49] Incandescent Reflector, https://www.infraphil.info/Philips_Infraphil-PAR38E.pdf (accessed 1 June 2021).
[50] J. Xu, K. Yao, Z. Xu, Nanomaterials with a photothermal effect for antibacterial activities: an overview, Nanoscale 11 (2019) 8680–8691, https://doi.org/10.1039/C9NR01833F.